Journal of Electron Microscopy **60(2)**: 101–108 (2011)
doi: 10.1093/jmicro/dfr002

Physical: Full-length

Estimation of wave fields of incident beams in a transmission electron microscope by using a small selected-area aperture

Shigeyuki Morishita[1,*,†], Jun Yamasaki[2] and Nobuo Tanaka[2]

[1]Department of Crystalline Materials Science, Nagoya University, Furo-cho, Nagoya 464-8603, Japan and [2]EcoTopia Science Institute, Nagoya University, Furo-cho, Nagoya 464-8603, Japan
*To whom correspondence should be addressed. E-mail: morishita@nagoya-u.jp
†Research Fellow of the Japan Society for the Promotion of Science, Japan.

Abstract The direction of an electron beam in a nanometer-sized area is measured directly by utilizing a selected-area aperture. By the measurements at several areas in a beam, the wavefront curvature and thus the defocus value of the beam are detected. From the defocus value, the wave field at the specimen plane is also reproduced in consideration of the influences of the condenser aperture and spherical aberration of the illumination lens. The result shows that phase deviation of 2π is caused only at about 10 nm apart from the beam center in a beam with a typical diameter for high-resolution transmission electron microscopy. Based on the defocus value, the convergence angle of the beam is also estimated to be about 6 mrad without being influenced by the partial coherence, that is, independently of the type of the electron gun. Measuring the defocus values for only two beam diameters enables us to determine geometrical parameters peculiar to the illumination system, based on which wave fields of any beam diameters by any condenser aperture sizes can be estimated. The technique proposed in this paper is effective in evaluating the influence of wavefront curvature of incident beams on various kinds of precise measurements conducted in transmission electron microscopes.

Keywords incident wave field, wavefront curvature, selected-area diffraction, transmission electron microscope, small selected-area aperture, incident angle

Received 25 November 2010, accepted 11 January 2011, online 13 February 2011

Introduction

Recent improvements in precision of structure analyses using transmission electron microscopes (TEM) have increased the importance of accurate evaluation of incident beam properties such as current density, wavelength, spatial and temporal coherence, and wavefront curvature. In various measurements in TEM such as high-resolution transmission electron microscopy (HRTEM) and selected-area diffraction, incident electron beams are generally assumed to be plane waves. In practice, incident beams are, however, required to be convergent/divergent in order to increase the current density at the specimen plane so that wavefronts of incident beams around the specimen plane are curved. This means that incident directions differ from position to position in the beam. The wavefront curvature results in a nonuniform phase of the incident wave at the specimen plane.

The wavefront curvature should influence results and interpretations in HRTEM with its resolution and data accuracy being improved by aberration corrections [1,2]. Also, the results and interpretations obtained by various methods, which deal with

complex wave fields, should be influenced by the wavefront curvature. Here, the various methods include electron holography [3], focal-series reconstruction of exit waves [4], transport of intensity equation (TIE) method [5] and electron diffractive imaging [6]. For example, it has been reported that position dependence of the point spread function in electron holography can be eliminated based on measurements of the wavefront curvatures of elliptical beams [7], although aberrations of the objective lens must be known accurately prior to the measurements. In this study, we propose a useful technique for measuring wavefront curvature utilizing a small selected-area aperture [8]. Although the technique can be applied for electron beams with arbitrary shapes, wavefront curvatures of usual round beams are measured in this study. Based on the results, we demonstrate reproduction of wave fields for the entire electron beams also considering diffraction from a condenser aperture.

Theory and method

As mentioned in the introduction, wavefronts of the incident electron beams are curved and their phase depends on a position in a two-dimensional specimen plane. Figure 1 shows a schematic of an illumination system with a point source. In Fig. 1, all lenses contributing to the formation of incident beams are represented as one illuminating lens, which includes the prefield of the objective lens. An electron beam emitted from the point source passes through the illumination system and forms a demagnified image of the source. When the focussing point of the source image is deviated from the specimen plane, a defocused image of the source is formed there. Here, the defocus value Δf is defined to be negative for underfocus. Let $\boldsymbol{r} = (r, \omega_r)$ and $\boldsymbol{q} = (q, \omega_q)$ be the polar coordinates in a specimen plane and a pupil plane, respectively, with their origins at the optical axis. Assuming a monochromatic point source, a wave function $\psi(\boldsymbol{r})$ of an incident round beam at the specimen plane is given by

$$\psi(\boldsymbol{r}) = F[A(\boldsymbol{q})\, \mathrm{e}^{-\mathrm{i}\chi(\boldsymbol{q})}] \tag{1}$$

with a condenser aperture function

$$A(\boldsymbol{q}) = \begin{cases} 1, & q \le \theta/\lambda, \\ 0, & q > \theta/\lambda \end{cases} \tag{2}$$

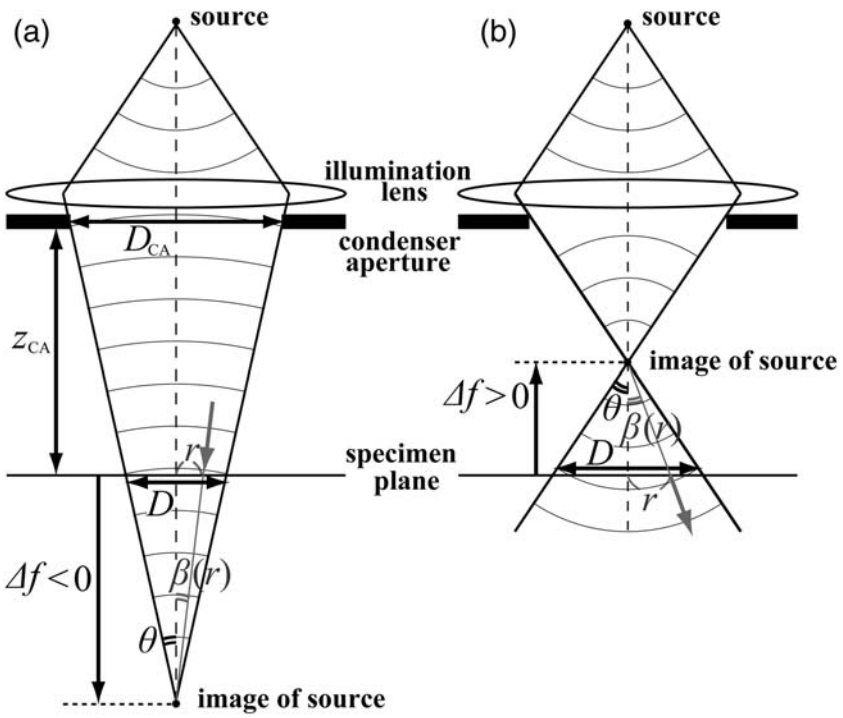

Fig. 1. Schematic of an illumination system consisting of a point source, an effective illumination lens and an effective condenser aperture. The diagram shows the case of (a) negative and (b) positive Δf, where D is the beam diameter, θ the convergence angle and $\beta(r)$ the incident angle at a position r away from the optical axis in the specimen plane.

and an aberration function of the illumination lens

$$\chi(\boldsymbol{q}) = \pi\lambda\Delta f q^2 + \tfrac{1}{2}\pi\lambda^3 C_s q^4, \quad (3)$$

where λ is the wavelength of electrons, θ the convergence semi-angle of the beam, C_s the spherical-aberration coefficient of the illumination lens and F the Fourier transform. These formulae are used to reproduce electron beams not only in TEM, but also in scanning transmission electron microscopy (STEM) and nano-beam diffraction (NBD), with beam diameters less than 100 nm [9]. For such smaller beam diameters, a condenser aperture with a diameter of 10–40 μm and $|\Delta f|$ much less than that for ordinary illuminating conditions in TEM are generally used. Since small values of $|\Delta f|$ make the contribution of the first term relatively small to the second term in Eq. (3), spherical aberration cannot be neglected without aberration correction. On the other hand, in TEM, an electron beam diameter larger than 100 nm is formed generally by a condenser aperture about 100 μm in diameter and much larger values of $|\Delta f|$ than those in STEM and NBD. Because of large values of $|\Delta f|$, the second term and other terms coming from higher-order aberrations omitted in Eq. (3) can be neglected, even if we use a condenser aperture 100 μm in diameter. Also Fresnel fringes caused by the condenser aperture can be neglected in the central area of the electron beam, since they generally appear only around the outer edge of the beam. In this study, we call the central area *inner area*, and the area which is outside of the inner area but is inside of the beam edge *rim area*. In the inner area, Eq. (1) becomes

$$\psi(\mathbf{r}) \cong F[\mathrm{e}^{-\mathrm{i}\pi\lambda\Delta f q^2}] \propto \mathrm{e}^{\mathrm{i}(\pi/\lambda\Delta f)r^2}. \quad (4)$$

This is identical with a spherical wave propagating from a point source located $|\Delta f|$ away [10]. In the inner area, as shown in Fig. 1, an incident angle $\beta(r)$ at the specimen plane depends on a position as

$$\beta(r) \cong \frac{r}{\Delta f}. \quad (5)$$

Measuring incident angles $\beta(r)$ at different positions determines the value of Δf and thus wavefront curvature in the inner area. In this study, the measurements are conducted by using a small selected-area aperture as described in detail later.

Experimental

We used a 200 kV thermal field-emission TEM (JEOL: JEM-2100F) equipped with an imaging aberration corrector (CEOS GmbH, CETCOR). The corrector is, however, not necessary for this study as described later. A nominal spherical-aberration coefficient of the objective prefield lens is 0.5 mm. The diameter of the condenser aperture used is 100 μm as in ordinary TEM observations. For selected-area diffraction, a small pinhole of 240 nm in diameter opened in a metallic thin plate was prepared by using focused ion beam (FIB) [6]. When inserted in the conjugate plane of the objective lens, it acts as an aperture to select a specimen area of about 3.0 nm in diameter as shown in Fig. 2a. The diffraction spot is naturally the Airy pattern, namely the Fraunhofer diffraction pattern from a circular aperture, as shown in Fig. 2b. Diffraction patterns were recorded on negative films at a nominal camera length of 200 cm, which was calibrated to the practical value based on a diffraction pattern of a silicon crystal.

Results and discussion

In our experiments, wavefront curvature was estimated by measuring incident directions by using the small selected-area aperture. When the aperture is inserted into a beam, the position of the direct spot in the diffraction pattern reflects the beam direction inside the aperture. Therefore, when we move the aperture or the beam, the direct spot

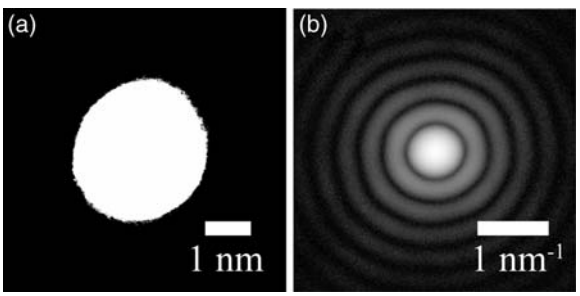

Fig. 2. (a) Selected-area aperture which selects an area of about 3 nm in diameter in the specimen plane. (b) Diffraction pattern from the aperture (Airy pattern) shown on a logarithmic scale in order to see the rings clearly.

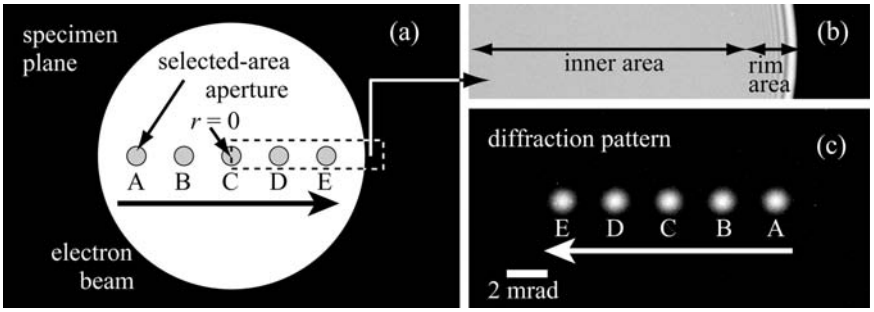

Fig. 3. (a) Schematic showing the specimen plane illuminated by an electron beam. Diffraction patterns are recorded at each position from A to E by the aperture in Fig. 2a. (b) TEM image of the electron beam. Incident angles are measured within the inner area in order to avoid the influence of Fresnel fringes in the rim area. (c) Shift of the direct spot shown on a linear scale when measured at the positions shown in (a).

shifts according to the wavefront curvature. The shifts of the spot positions were measured for round electron beams with a diameter D of 140, 280, 560, 840 and 1120 nm. To avoid the influence of off-axis aberrations of the imaging lenses, the small selected-area aperture was fixed on the optical axis and electron beams were moved by a double deflection coil system. The relative position of the aperture to a beam was shifted from A to E at regular intervals as shown in Fig. 3a. To avoid the influence of Fresnel fringes around the beam edge, only the inner area as shown in Fig. 3b was used for the measurements.

Figure 3c shows the shift of the direct spot recorded by multi-exposures while a beam of 560 nm in diameter at $\Delta f < 0$ is shifted at 120 nm intervals. Since the intensity of the spots is shown on a linear scale, only the main peak of each Airy pattern is visible in the figure. The measurement is plotted in Fig. 4. From the gradient $\beta(r)/r$ of the plot and Eq. (5), the defocus Δf is estimated to be −45 μm. As shown in Fig. 1, a convergence semi angle is expressed as follows:

$$\theta \cong \frac{D}{2|\Delta f|}, \tag{6a}$$

$$\theta \cong \frac{D_{\mathrm{CA}}}{2(z_{\mathrm{CA}} - \Delta f)}. \tag{6b}$$

Substituting $\Delta f = -45$ μm and $D = 560$ nm into Eq. (6a) gives the convergence angle $\theta = 6.3$ mrad. The same measurements were conducted for various beam diameters D at $\Delta f < 0$. The results are summarized in Fig. 4 and Table 1. The effective condenser aperture shown in Fig. 1 is a demagnified image of the actual condenser aperture. Assuming that a second condenser lens is a thin lens, which is used for changing the beam diameter, the distance from the specimen plane z_{CA} and the diameter D_{CA} of the effective condenser aperture are independent of the beam diameter. Fitting Eq. (6b) to Δf and θ in Table 1 results in $D_{\mathrm{CA}} = 14 \pm 2$ μm and $z_{\mathrm{CA}} = 1.1 \pm 0.2$ mm.

We estimated additional beam tilts induced during the beam shifts by the double deflection coils. Owing to the inversion of the wavefront

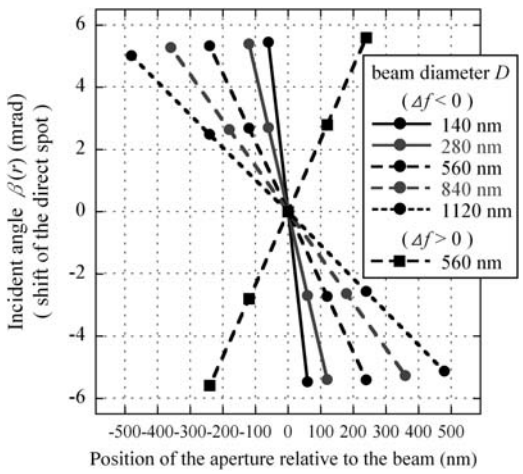

Fig. 4. Shifts of the direct spot as the functions of the aperture positions relative to the beams. The incident angle at the optical axis is set to be zero.

Table 1. Measured defocus Δf and convergence semi angle θ of the beams with different diameters D

D (nm)	Δf (μm)	θ (mrad)
140	−11.0 ± 0.6	6.4 ± 0.3
280	−22 ± 1	6.3 ± 0.3
560	−45 ± 2	6.3 ± 0.3
840	−69 ± 3	6.1 ± 0.3
1120	−95 ± 5	5.9 ± 0.3

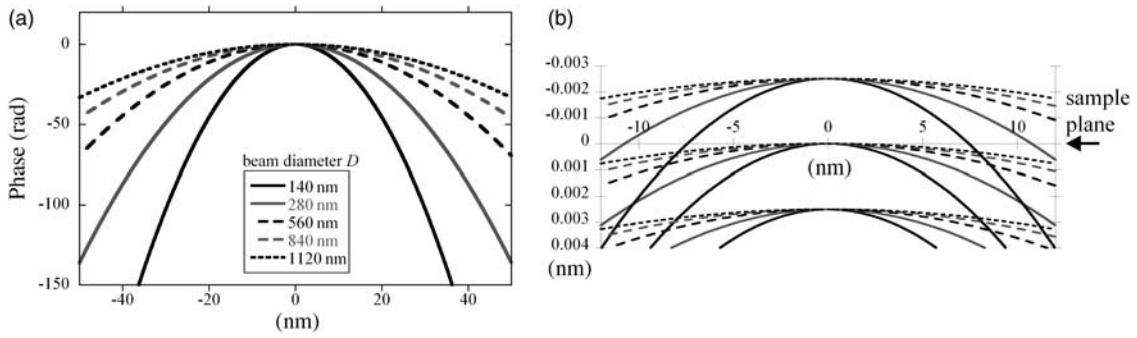

Fig. 5. (a) Phase distributions of incident waves at the specimen plane. (b) Wavefront curvature around the specimen plane. (a) and (b) are calculated by substituting measured Δf shown in Table 1 into Eqs. (4) and (7), respectively. Because the wavelength of the electron beams is short, the diagram of the wavefronts (b) is enlarged in the optical axis direction.

curvatures, opposite signs of Δf cause shifts of direct spot into opposite directions, while the additional tilt by the deflection coils occurs regardless of sign of Δf. Therefore, if we compare the results at $\pm\Delta f$ in Fig. 4, then the additional tilt can be estimated. For the beam diameter $D = 560$ nm, the positive value of Δf is calculated to be +43 μm from Eqs. (6a) and (6b). Then Eq. (5) gives the total shift of the direct spot for beam shift of 480 nm as 11.5 mrad, which is measured to be 11.2 mrad in Fig. 4. The slight difference results from the additional tilt. This effect is regarded as errors denoted in Table 1.

As shown in Fig. 5a, phase distributions at the specimen plane are calculated by substituting Δf and θ in Table 1 into Eq. (4). Assuming that the curved wavefronts appear around the specimen plane at intervals of the wavelength λ along the optical axis, the wavefronts at a certain time are denoted by a formula

$$z = -\frac{r^2}{2\Delta f} + n\lambda + \varphi, \quad \text{where } n \text{ is an integer,} \quad (7)$$

where z is the coordinate along the optical axis and ϕ the arbitrary constant phase. Wavefronts shown in Fig. 5b are calculated by entering Δf in Table 1 into the formula. Comparison between Figs 4 and 5 shows that only a few mrad of changes in the incident angle induce significant changes in phase at the specimen plane because of the short wavelength of 200 kV electron beams. For example, when we perform HRTEM using an electron beam 280 nm in diameter, the phase shift of 2π occurs only at 10.5 nm apart from the optical axis. Such large phase shifts and corresponding tilt angles should require attention in interpreting data in various kinds of precise measurements.

In typical HRTEM conditions, maximum tilt angles are at most 6 mrad at beam edges as shown in Table 1. According to the previous research [11], an incident angle of 2° (35 mrad) with respect to the optical axis has little influence on aberration-corrected HRTEM images of a GaP crystal taken from a [1 1 0] direction. Therefore, the wavefront curvature of incident beams has little influence on HRTEM images of zincblende or diamond structures from the [1 1 0] direction. Although the degree of the influence may depend on crystalline structures, HRTEM images of other crystal structures are presumed to be little affected by the wavefront curvature. Similar careful evaluations of the influence of the wavefront curvature should also be done for results of various kinds of phase reconstruction methods.

So far, we have analyzed the wave fields only in the inner area by neglecting the spherical aberration of the illumination lens and Fresnel diffraction from the condenser aperture. Here we take account of them and evaluate both the inner and rim areas quantitatively. Figure 6a compares amplitude profiles of incident waves calculated by Eqs. (1) and (4) for $D = 280$ nm, where $\Delta f = -22$ μm and $\theta = 6.3$ mrad. Effects of the spherical aberration ($C_s = 0.5$ mm) and the condenser aperture are considered in the former (black line) and neglected in the latter (horizontal gray dashed line). Although the black line has oscillations in the rim area, it coincides with the gray dashed profile in the inner area shown by the arrow. Figure 6b shows differences of

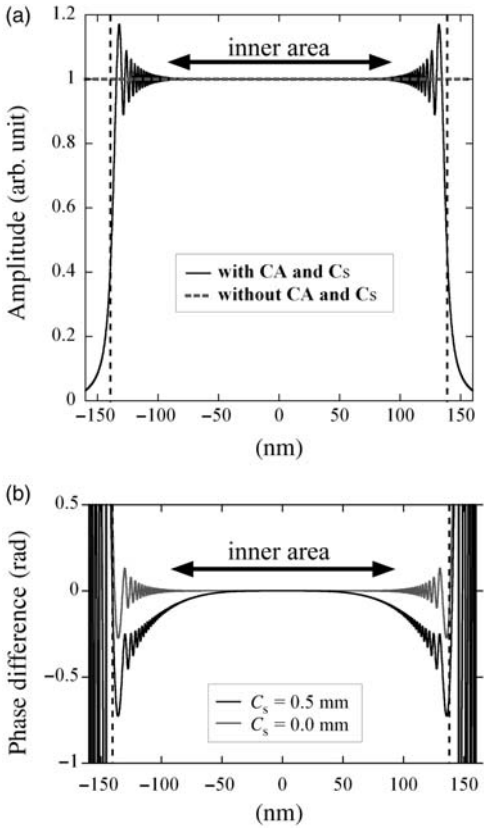

Fig. 6. (a) Amplitude profiles of an incident beam 280 nm in diameter calculated by Eqs. (1) and (4), where $\Delta f = -22$ μm, $C_s = 0.5$ mm, and $\theta = 6.3$ mrad. Effects of the condenser aperture (CA) and the spherical aberration (C_s) are considered in the profile obtained from Eq. (1) and neglected in the profile obtained from Eq. (4). In order to simulate realistic incident wave fields, an edge of a condenser aperture is blurred slightly in the calculations. (b) Profiles of phase difference with and without the effect of the condenser aperture. For comparison, the black line profile is obtained by setting $C_s = 0.5$ mm in Eq. (1) and the gray line profile is obtained by $C_s = 0.0$ mm in Eq. (1). The vertical broken black lines show the beam diameter of 280 nm.

the phases calculated by both Eq. (4) shown in Fig. 5 and Eq. (1). For comparison, the two profiles in Fig. 6b are obtained by setting $C_s = 0.5$ and 0.0 mm in Eq. (1), respectively. Oscillation of phases caused by the condenser aperture appears only in the rim area like the amplitudes in Fig. 6a. Although the phase shifts caused by the spherical aberration occur also in the inner area, they are negligibly small as compared to those by defocus (Fig. 5a). These results mean that wave fields based on Eq. (4) are valid in the inner area from viewpoints of both amplitude and phase.

As shown in Fig. 6a, beams used in general TEM observations have inner areas, the extent of which depends on Δf. When $|\Delta f|$ decreases, the inner area shrinks with decreasing beam diameter. Even if Δf is fixed, the diameter of the beam and thus also the inner area are reduced when the condenser aperture is exchanged with a smaller one. Therefore, the inner area almost disappears in NBD, in which a beam diameter less than 100 nm is generally formed by a condenser aperture 10–40 μm in diameter. Although such beams have been often used for precise experiments such as electron diffractive imaging [12], the fluctuating amplitude should require additional complicated procedures for data analyses and may reduce the accuracy of the experimental results in electron diffractive imaging. From this point of view, selected-area nano-diffraction (SAND) should be the most appropriate technique to record accurate and precise diffraction patterns from nanometer-sized areas [6,8]. For uniform illumination in terms of amplitude and phase, an object should be located in the inner area formed by a large condenser aperture, for example, 100 μm in diameter. Then, a part of the inner area including the object can be selected by a small aperture as shown in Fig. 2a in an aberration-corrected TEM.

In this study, we did not deal with coherence of incident beams, which is a different parameter from the wavefront curvature. When electrons come not from a point source but from an extended source, the beam is partially spatially coherent. When electrons are not monochromatic, the beam is partially temporally coherent. In both cases, the electrons come to the same position in a specimen plane with different incident directions. Thus, partial coherence of electron beams results in blurring of diffraction patterns. When no selected-area aperture is inserted, radii of the diffraction disks are sum of the convergence semi angle θ and the blurring angle, if we set the diffraction focus on the back-focal plane exactly. In the case of a thermal LaB_6 filament, the present method could be the best way to estimate θ. On the other hand, θ in a field emission TEM can be measured also from the disk radius with the same precision to the present technique, because the influence of the partial coherence can be almost neglected. To be precise, also the direct spots in Figs 2b and 3c should be slightly blurred. However, only the peak positions are important for the measurements of the incident directions. Thus, the influence of the partial

coherence can be neglected in the present technique, even if we use a thermal LaB_6 filament. The influence of the coherence could appear significantly in the rim area. Intensity profiles including oscillation in the rim area shown in Fig. 6 may change because of the partial coherence, especially in the case of a thermal LaB_6 filament.

The most significant feature of the present technique is a direct measurement of wavefront curvature of electron wave fields. One of the applications of the direct measurement of local beam directions may be precise beam alignment. As is often the case with HRTEM observations, undesirable beam tilt is generally caused at the center of the field of view, when we change the diameter of the electron beam. The resultant misalignment for voltage center can be detected directly and compensated by using the present method. In the present study, we demonstrated the reproduction of wave fields on the basis of one-dimensional measurements of wavefront curvature by assuming a round beam. It should also be possible that wave fields of electron beams with arbitrary shapes, for example, elliptical beams used in electron holography, are examined two dimensionally with the spatial resolution of 3 nm by the technique.

In this study, an electron microscope equipped with an imaging aberration corrector was used. It is known well in textbooks that area-selection errors of $C_{\text{s-post}}\alpha^3$ ($C_{\text{s-post}}$ is the spherical-aberration coefficient of the objective postfield lens and α the diffracted angle) are caused in the selected-area diffraction. When we use a converging or diverging beam instead of parallel illumination, the tilt angle β naturally turns out to be the effective diffracted angle α. If we calculate the error for $C_{\text{s-post}} = 0.5$ mm and $\alpha = 6.0$ mrad, then it is only 0.1 nm which is much smaller than the beam shifts in our measurements. Thus, the measurements in Fig. 4 are easily conducted with a sufficiently high accuracy in any TEM instruments without an aberration corrector, only if a small aperture has been equipped. In principle, measurements for only two kinds of beam diameters are enough for estimating D_{CA} and z_{CA}, though we measured six kinds of diameters in Fig. 5. If once estimated, then Eqs. (6a) and (6b) give Δf and θ for any beam diameters and thus the corresponding wave fields as shown in Figs. 6a and b without any experiments. This technique should be useful for evaluating the effects of curved incident waves on various kinds of precise measurements conducted in TEM.

Conclusion

We propose a technique to estimate incident wave fields at the specimen plane in TEM. The local incident directions in an electron beam are measured by a selected-area aperture of effectively 3 nm in diameter through the detection of shifts of the direct spot. Based on the measurement results, the incident wave fields are reproduced. It was confirmed that phase shift of 2π occurs at only about 10 nm apart from the optical axis in a beam generally used in HRTEM. Although having little influence on HRTEM images of GaP, such large phase shifts and corresponding incident angles may require attention in interpreting data in HRTEM and various kinds of phase reconstruction methods such as holography.

Measuring incident angles for only two beam diameters enables us to determine the distance from the specimen plane and the diameter of the effective condenser aperture. Using the two parameters, incident wave fields of any beam diameters by any condenser aperture sizes can be estimated without any experiments. Thus, the measurements are easily conducted with a sufficiently high accuracy in any TEM instruments, only if a small aperture has been installed.

The most significant feature of the present technique is a direct measurement of wavefront curvature of electron wave fields. In this study, we demonstrated the reproduction of wave fields on the basis of one-dimensional measurements of wavefront curvature by assuming a round beam. It should also be possible that wave fields of electron beams with arbitrary shapes, for example, elliptical beams used in electron holography, are examined two-dimensionally with the spatial resolution of 3 nm by the technique. In future, characterization of the influence of curved incident waves on various kinds of measurement will improve the precision of the measurement.

Funding

This work was partly supported by Grant-in-Aid for Scientific Research on Priority Areas (grant number

18029011) from The Ministry of Education, Culture, Sports, Science and Technology; Grant-in-Aid for Young Scientists (B) (grant number 21760026) and Grant-in-Aid for JSPS Fellows (grant number 226455) from Japan Society for the Promotion of Science.

Acknowledgements

The authors are most grateful to Dr T. Kato of Japan Fine Ceramics Center for producing the selected-area aperture. The authors also would like to thank Dr H. Sawada, Dr S. Ohta and Mr T. Tomita of JEOL Ltd for their valuable advice on instruments, and to Mr T. Nambara of NIDEC Co. Ltd for helpful discussion about optics.

References

1 Haider M, Rose H, Uhlemann S, Kabius B, and Urban K (1998) Towards 0.1 nm resolution with the first spherically corrected transmission electron microscope. *J. Electron Microsc.* **47**: 395–405.

2 Yamasaki J, Kawai T, Kondo Y, and Tanaka N (2008) A practical solution for eliminating artificial image contrast in aberration-corrected TEM. *Microsc. Microanal.* **14**: 27–35.

3 Lehmann M and Lichte H (2005) Electron holographic material analysis at atomic dimensions. *Cryst. Res. Technol.* **40**: 149–160.

4 Thust A, Overwijk M H F, Coene W M J, and Lentzen M (1996) Numerical correction of lens aberrations in phase-retrieval HRTEM. *Ultramicroscopy* **64**: 249–264.

5 Volkov V V, Zhu Y, and De Graef M (2002) A new symmetrized solution for phase retrieval using the transport of intensity equation. *Micron* **33**: 411–416.

6 Morishita S, Yamasaki J, Nakamura K, Kato T, and Tanaka N (2008) Diffractive imaging of the dumbbell structure in silicon by spherical-aberration-corrected electron diffraction. *Appl. Phys. Lett.* **93**: 183103.

7 Lehmann M (2004) Influence of the elliptical illumination on acquisition and correction of coherent aberrations in high-resolution electron holography. *Ultramicroscopy* **100**: 9–23.

8 Yamasaki J, Sawada H, and Tanaka N (2005) First experiments of selected area nano-diffraction from semiconductor interfaces using a spherical aberration corrected TEM. *J. Electron Microsc.* **54**: 123–126.

9 Zuo J M, Gao M, Tao J, Li B Q, Twesten R, and Petrov I (2004) Coherent nano-area electron diffraction. *Microsc. Res. Tech.* **64**: 347–355.

10 Born M and Wolf E (1999) *Principles of Optics*, 7th edn (Cambridge University Press, Cambridge).

11 Tanaka N, Yamasaki J, Fuchi S, and Takeda Y (2004) First observation of $In_xGa_{1-x}As$ quantum dots in GaP by spherical-aberration-corrected HRTEM in comparison with ADF-STEM and conventional HRTEM. *Microsc. Microanal.* **10**: 139–145.

12 Zuo J M, Vartanyants I, Gao M, Zhang R, and Nagahara L A (2003) Atomic resolution imaging of a carbon nanotube from diffraction intensities. *Science* **300**: 1419–1421.